Molecular squares of Ni^{II} and Cu^{II}: ferromagnetic exchange interaction mediated by *syn–anti* carboxylate-bridging†

Himanshu Arora,[a] Francesc Lloret[b] and Rabindranath Mukherjee*[a]

Received 18th March 2009, Accepted 4th September 2009
First published as an Advance Article on the web 28th September 2009
DOI: 10.1039/b905463d

The synthesis of four discrete tetranuclear complexes $\{[Ni^{II}(L^2)][ClO_4]\}_4\cdot MeCN$ (**1**), $\{[Cu^{II}(L^1)(O_3SCF_3)]\}_4\cdot H_2O$ (**2**), $\{[Cu^{II}(L^3)(OClO_3)]\}_4\cdot MeCN$ (**3**) and $\{[Cu^{II}(L^4)][ClO_4]\}_4\cdot 3MeCN\cdot 4H_2O$ (**4**), supported by a closely similar group of carboxylate–appended (2–pyridyl)alkylamine ligands [$L^1(-)$: 3-[*N*-methyl-{2-(pyridin-2-yl)ethyl}amino]propionate; $L^2(-)$: 3-[(2-(pyridin-2-yl)ethyl){2-(pyridin-2-yl)methyl}amino]propionate; $L^3(-)$: 3-[*N*-isopropyl-{2-(pyridin-2-yl)methyl}amino]propionate and $L^4(2-)$: 3-[*N*-{2-(pyridin-2-yl)methyl}amino]-bis(propionate)] is described. Structural characterization reveals that each Ni^{II} centre in **1** has square-pyramidal $Ni^{II}N_3O_2$ coordination and each Cu^{II} centre in **2–4** has distorted square-pyramidal $Cu^{II}N_2O_3$ coordination, utilizing three N and one carboxylate O in **1** and two N and carboxylate O (one in **2** and **3**; two in **4**) of the ligand and the fifth/fourth coordination is provided by an oxygen atom belonging to the carboxylate group of an adjacent molecule. A $CF_3SO_3^-$ or a ClO_4^- ion provides an O coordination in **2** and **3**, respectively. Temperature-dependent magnetic studies reveal the existence of ferromagnetic exchange interaction in each case, due to the presence of equatorial–equatorial *syn–anti* carboxylate bridge between M^{II} centres.

Introduction

Magnetostructural studies on polynuclear complexes, aimed at understanding the underlying structural factors that govern the magnetic exchange interaction between paramagnetic centres mediated by ligand bridge(s), continue to be of interest.[1–3] Polynuclear metal carboxylates[4] are good candidates for the investigation of the magnetic exchange interaction between adjacent metal ions. Carboxylate groups can assume many types of bridging conformations, the most important being triatomic *syn–syn*, *syn–anti*, *anti–anti* and monoatomic.[5,6] *Syn–syn* conformation favours the generation of binuclear systems whereas *syn–anti* favours the formation of extended structures with varying nuclearity. The former mediates the antiferromagnetic exchange pathway between the metal centres, while the latter favours ferromagnetic exchange interaction with some exceptions where antiferromagnetic coupling is favoured.[7] It is well known that the carboxylate group can bridge metal ions to give rise to a variety of polynuclear transition metal complexes, ranging from discrete entities to three-dimensional systems.[7–9]

From the perspective of generating discrete closed oligomeric structures we have chosen the carboxylate-appended (2-pyridyl)-alkylamine ligands. In fact, very recently we have shown[10] that the carboxylate-appended anionic (2-pyridyl)alkylamine ligands afforded 1D coordination polymers of Co^{II} and Cu^{II} supported by $L^2(-)$ and a discrete Cu^{II}_4 cluster supported by $L^1(-)$, providing examples of ligand denticity-controlled self-assembly process. Temperature-dependent magnetic susceptibility measurements revealed (i) spin-canted antiferromagnetism in 1D coordination polymer of Co^{II}, (ii) weak antiferromagnetic exchange interaction in 1D coordination polymer of Cu^{II} and (iii) ferromagnetic exchange interaction in tetracopper(II) complex. Hoping that synthetic generality of the formation of M^{II}_4 core supported by carboxylate-appended anionic (2-pyridyl)-alkylamine ligands could be established and from the aforesaid perspective in this work we have included two new (2-pyridyl)-alkylamine-based ligands [lithium salts of 3-[*N*-isopropyl-{2-(pyridin-2-yl)methyl}amino]propionate $L^3(-)Li^+$ and 3-[*N*-{2-(pyridin-2-yl)methyl}amino]-bis(propionate) $\{L^4(2-)(2Li^+)\}$ with flexible carboxylate linker. Specifically, we have synthesized four discrete tetranuclear complexes $\{[Ni^{II}(L^2)][ClO_4]\}_4\cdot MeCN$ (**1**), $\{[Cu^{II}(L^1)(O_3SCF_3)]\}_4\cdot H_2O$ (**2**), $\{[Cu^{II}(L^3)(OClO_3)]\}_4\cdot MeCN$ (**3**) and $\{[Cu^{II}(L^4)][ClO_4]\}_4\cdot 3MeCN\cdot 4H_2O$ (**4**), with closely similar metal–ligand bonding characteristics. We present here the magnetostructural behaviour of these complexes.

Experimental

General considerations

All reagents and solvents were obtained from commercial sources and used as received. Solvents were dried/purified following standard procedures. $L^1(-)Li^+$ and $L^2(-)Li^+$ were prepared as before.[10] The methodology followed to prepare the new ligands $L^3(-)Li^+$ and $\{L^4(2-)(2Li^+)\}$ was adapted from reported procedures.[10,11]

[a]*Department of Chemistry, Indian Institute of Technology Kanpur, Kanpur, 208 016, India. E-mail: rnm@iitk.ac.in; Fax: +91 512 2597436; Tel: +91 512 2597437*

[b]*Instituto de Ciencia Molecular (ICMol), Universidad de València, Polígono de la Coma, s/n, 46980-, Paterna, València, Spain*

† Electronic supplementary information (ESI) available: Absorption spectra of complexes (Fig. S1–S4); X-ray structure of **3** (Fig. S5); C–H···π interaction in **1** (Fig. S6) and C–H···O interaction in **3** (Fig. S7); C–H···π and C–H···O parameters for **1**, **2** and **3** (Table 1). CCDC reference numbers 718562–718564. For ESI and crystallographic data in CIF or other electronic format see DOI: 10.1039/b905463d

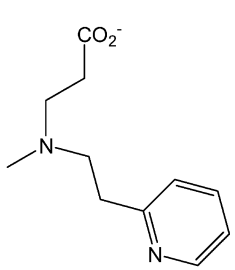

$L^1(-)$

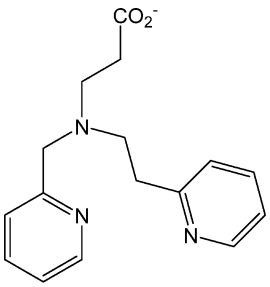

$L^2(-)$

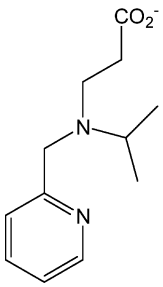

$L^3(-)$

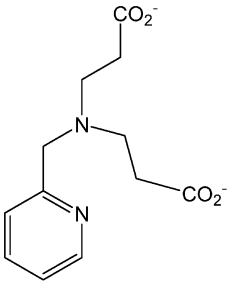

$L^4(2-)$

Synthesis of lithium salt of 3-[*N*-isopropyl-{2-(pyridin-2-yl)methyl}amino]-propionate {$L^3(-)Li^+$}. Isopropylamine (2.00 g, 0.034 mol) and pyridin-2-carbaldehyde (3.67 g, 0.034 mol) were mixed in dry MeOH (20 mL) and the reaction mixture was stirred for 3 h. During addition, the temperature was maintained below 10 °C. To the above stirred solution, an aqueous solution of $NaBH_4$ (3.05 g, 0.085 mol) which contains NaOH (2.04 g, 0.051 mol) was added dropwise. The reaction mixture was allowed to stir for ~12 h. The volume of the reaction mixture was reduced to half of its original volume and then it was extracted using CH_2Cl_2 and finally washed with brine water. The organic layer was dried over anhydrous Na_2SO_4. Removal of solvent was removed under vacuum to give a yellow oil of *N*-(pyridin-2-ylmethyl)propan-2-amine (yield: 3.61 g, 70%). ^{1}H NMR (80 MHz; $CDCl_3$): $\delta = 8.30$ (d, 1 H, py-H^6), 7.50–6.90 (m, 3 H, py-$H^{3,4,5}$), 3.89 (s, 2 H, CH_2py), 2.25 (m, 1 H, CH(CH_3)$_2$), 1.05 (d, 6 H, CH(CH_3)$_2$).

N-(pyridin-2-ylmethyl)propan-2-amine (2.00 g, 0.013 mol) and methyl acrylate (1.14 g, 0.013 mol) were mixed in dry MeOH (20 mL) and the reaction mixture was refluxed for 24 h. The solvent was removed under vacuum to give a yellow-brown oil of methyl-3-{isopropyl(pyridin-2-ylmethyl)amino}propionate (yield: 2.32 g, 75%). ^{1}H NMR (80 MHz; $CDCl_3$): $\delta = 8.30$ (d, 1 H, py-H^6), 7.50-6.90 (m, 3 H, py-$H^{3,4,5}$), 3.79 (s, 2 H, CH_2py), 3.63 (s, 3 H, $CH_2CH_2CO_2CH_3$), 2.95–2.45 (m, 4 H, CH_2CH_2CO$_2$CH$_3$), 2.25 (m, 1 H, CH(CH_3)$_2$), 1.05 (d, 6 H, CH(CH_3)$_2$).

Methyl-3-{isopropyl(pyridin-2-ylmethyl)amino}propionate (2.32 g, 0.010 mol) was redissolved in dry MeOH (20 mL) and to it solid LiOH (0.25 g, 0.010 mol) was added. After stirring for 2 d, the solvent was removed under vacuum to give a pale yellow oil of lithium salt of 3-{isopropyl(pyridine-2-ylmethyl)amino}propionate {($L^3(-)Li^+$} (yield: 1.38 g, 60%). ^{1}H NMR (80 MHz; $CDCl_3$): $\delta = 8.30$ (d, 1 H, py-H^6), 7.50-6.90 (m, 3 H, py-$H^{3,4,5}$), 3.79 (s, 2 H, CH_2py), 2.95–2.45 (m, 4 H, CH_2CH_2CO$_2^-$), 2.25 (m, 1 H, CH(CH_3)$_2$), 1.05 (d, 6 H, CH(CH_3)$_2$).

Synthesis of lithium salt of 3-[*N*-{2-(pyridin-2-yl)methyl}amino]-bis(propionate) {$L^4(2-)(2Li^+)$}. Pyridin-2-yl-methanamine (2.00 g, 0.019 mol) and methyl acrylate (3.27 g, 0.038 mol) were mixed in dry MeOH (20 mL) and the reaction mixture was refluxed for 24 h. The solvent was then removed under vacuum to give a yellow oil. The crude product was then subjected to column chromatography using $CHCl_3$/*n*-hexane (1 : 10) as eluent (yield: 3.25 g, 60%). ^{1}H NMR (80 MHz; $CDCl_3$): $\delta = 8.52$ (d, 1 H, py-H^6), 7.79–7.08 (m, 3 H, py-$H^{3,4,5}$), 3.76 (s, 2 H, pyCH_2), 3.65 (s, 6 H, $CH_2CH_2CO_2CH_3$), 2.91–2.35 (m, 8 H, CH_2CH_2CO$_2$CH$_3$).

L^4Me_2 (3.25 g, 0.012 mol) was redissolved in dry MeOH (20 mL). To it solid LiOH (0.58 g, 0.024 mol) was added and the reaction mixture was stirred for 2 d. The solvent was then removed under vacuum to give a pale yellow oil (yield: 1.88 g, 60%). ^{1}H NMR (80 MHz; $CDCl_3$): $\delta = 8.52$ (d, 1 H, py-H^6), 7.79-7.08 (m, 3 H, py-$H^{3,4,5}$), 3.76 (s, 2 H, pyCH_2), 2.91–2.35 (m, 8 H, CH_2CH_2CO$_2^-$).

Synthesis of {$[Ni^{II}(L^2)][ClO_4]$}$_4$·MeCN (1). To an aqueous solution (8 mL) of $L^2(-)Li^+$ (0.10 g, 0.35 mmol) solid $[Ni^{II}(H_2O)_6][ClO_4]_2$ (0.13 g, 0.35 mmol) was added. After refluxing for 3 h the reaction mixture was kept for slow evaporation. After a few days a blue crystalline compound was obtained. Recrystallization was achieved from DMF/MeCN/Et_2O vapour diffusion (yield: 0.12 g, 70%). Found: C 46.01, H 3.87, N 10.89. Calcd for $C_{72}H_{84}Cl_4N_{16}Ni_4O_{24}$: C 44.67, H 4.34, N 11.58%. Molar conductance, Λ_M (MeCN, ~1 mM, 298 K) = 430 Ω^{-1} cm^2 mol^{-1} (expected range[12] for 1 : 4 electrolyte: 410–460 Ω^{-1} cm^2 mol^{-1}). IR (KBr, cm^{-1}, selected peaks): 1610 (ν_{asymm}(CO)), 1445 (ν_{symm}(CO)) of carboxylate; 1092 and 623 (ν(ClO_4^-)). UV-vis (MeCN), λ_{max}/nm (ε/dm^3 mol^{-1} cm^{-1}): 910 (60) [ν_1 transition: $^3A_{2g} \rightarrow {}^3T_{2g}$ (octahedral parentage)],[13] 580 (100) [ν_2 transition: $^3A_{2g} \rightarrow {}^3T_{1g}$(F)], 370 sh (180) [$\nu_3$ transition: $^3A_{2g} \rightarrow {}^3T_{1g}$(P)], 260 (25 400).

{$[Cu^{II}(L^1)(O_3SCF_3)]$}$_4$·H_2O (2). To an aqueous solution (8 mL) of $L^1(-)Li^+$ (0.10 g, 0.47 mmol) solid $[Cu^{II}(H_2O)_6][CF_3SO_3]_2$ (0.21 g, 0.47 mmol) was added once at a time. The reaction mixture was refluxed for 2 h. Then it was kept for slow evaporation. After a few days, a blue crystalline compound was obtained, which was recrystallized using MeCN/Et_2O vapour diffusion (yield: 0.15 g, 75%). Found C 32.81, H 3.87, N 6.19. Calcd for $C_{48}H_{62}Cu_4F_{12}N_8O_{24}S_4$: C 33.00, H 3.55, N 6.42%. Molar conductance, Λ_M (MeCN, ~1 mM, 298 K) = 400 Ω^{-1} cm^2 mol^{-1}. IR (KBr, cm^{-1}, selected peaks): 1612 (ν_{asymm}(CO)), 1448 (ν_{symm}(CO)) and 1323 [ν_{asymm}(O_3SCF_3)], 1029 [ν_{symm}(O_3SCF_3)]; 1243 [ν_{asymm}(O_3SCF_3)], 1170 [ν_{symm}(O_3SCF_3)]. UV-vis (MeCN), λ_{max}/nm (ε/dm^3 mol^{-1} cm^{-1}): 638 (610) [support the presence of distorted octahedral stereochemistry; also true for **3** and **4** (see below)],[10] 290 sh (25 200), 260 (67 900).

{$[Cu^{II}(L^3)(OClO_3)]$}$_4$·MeCN (3). $L^3(-)Li^+$ (0.10 g, 0.44 mmol) and $[Cu^{II}(H_2O)_6][ClO_4]_2$ (0.16 g, 0.44 mmol) were mixed in water (8 mL) and the mixture was refluxed for 2 h. Then it was kept for slow evaporation. After a few days, it yielded a blue crystalline compound, which was recrystallized using MeCN/Et_2O vapour diffusion (yield: 0.14 g, 75%). Found C 39.01, H 3.87, N 10.19. Calcd for $C_{56}H_{68}Cl_4Cu_4N_{12}O_{24}$: C 39.78, H 4.02, N 9.94%. Molar conductance, Λ_M (MeCN, ~1 mM, 298 K) = 400 Ω^{-1} cm^2 mol^{-1}. IR (KBr, cm^{-1}, selected peaks): 1613 (ν_{asymm}(O_2CMe)), 1432 (ν_{symm}(O_2CMe)); 1115 and 623 (ν(ClO_4^-)).

Table 1 Data collection and structure refinement parameters for $\{[Ni^{II}(L^2)][ClO_4]\}_4\cdot MeCN$ (**1**), $\{[Cu(L^1)(O_3SCF_3)]\}_4\cdot H_2O$ (**2**), $\{[Cu(L^3)(OClO_3)]\}_4\cdot MeCN$ (**3**)

	1	**2**	**3**
Empirical formula	$C_{72}H_{84}Cl_4Ni_4N_{16}O_{24}$	$C_{48}H_{60}Cu_4F_{12}N_8O_{24}S_4$	$C_{56}H_{68}Cl_4Cu_4N_{12}O_{24}$
FW/g mol^{-1}	1934.19	1743.44	1689.18
Crystal system	Tetragonal	Tetragonal	Tetragonal
Space group	$P4_2/n$	$I\bar{4}$	$P42_1c$
a/Å	17.656(5)	19.7752(8)	20.532(5)
b/Å	17.656(5)	19.7752(8)	20.532(5)
c/Å	13.203(5)	8.4849(7)	8.217(5)
α/°	90	90	90
β/°	90	90	90
γ/°	90	90	90
V/Å^3	4116(2)	3318.1(3)	3464(2)
Z	2	2	2
Cryst size/mm^3	$0.20\times0.10\times0.10$	$0.13\times0.08\times0.07$	$0.10\times0.20\times0.20$
T/K	293(2)	100(2)	293(2)
λ/Å	0.71069	0.71073	0.71069
ρ_{calcd}/g cm^{-3}	1.561	1.745	1.619
μ/mm^{-1}	1.116	1.506	1.451
R_1,[a] wR_2[b]	0.0589, 0.1302	0.0369, 0.0919	0.0473, 0.1044
Goodness of fit	1.029	1.060	0.995
Parameters/restraints	272/0	227/3	246/2
N_{obs}, N_{unique}, R_{int}	26 849/5117/0.0762	10 684/3988/0.0313	23 088/4296/0.0820
Absolute structure parameter	—	0.046(16)	0.00(3)

[a] $R_1 = \Sigma(|F_o| - |F_c|)/\Sigma|F_o|$. [b] $wR_2 = \{\Sigma[w(|F_o|^2 - |F_c|^2)^2]/\Sigma[w(|F_o|^2)^2]\}^{1/2}$.

UV-vis (MeCN), λ_{max}/nm (ε/dm^3 mol^{-1} cm^{-1}): 640 (800), 290 sh (9500), 260 (23 400).

$\{[Cu^{II}(L^4)][ClO_4]\}_4\cdot 3MeCN\cdot 4H_2O$ (4). To an aqueous solution (10 mL) of $\{L^4(2-)(2Li^+)\}$ (0.10 g, 0.38 mmol) solid $[Cu^{II}(H_2O)_6][ClO_4]_2$ (0.14 g, 0.38 mmol), was added. The reaction mixture was refluxed for 2 h and then it was kept for slow evaporation. After a few days, it yielded a blue crystalline compound. Recrystallization was achieved by MeCN/Et_2O vapour diffusion (yield: 0.13 g, 75%). Found C 33.71, H 3.87, N 7.19. Calcd for $C_{54}H_{73}Cl_4Cu_4N_{11}O_{36}$: C 35.58, H 4.01, N 8.46%. Molar conductance, Λ_M (MeCN, ~1 mM, 298 K) = 400 Ω^{-1} cm^2 mol^{-1}. IR (KBr, cm^{-1}, selected peaks): 1701 (ν_{asymm} (O_2CMe), 1611 (ν_{asymm}(O_2CMe)), 1448 (ν_{symm}(O_2CMe)); 1103 and 625 (ν(ClO_4^-)). UV-vis (MeCN), λ_{max}/nm (ε/dm^3 mol^{-1} cm^{-1}): 620 (580), 280 sh (15 800), 257 (40 200).

Physical measurements

Elemental analyses were obtained using a Thermo Quest EA 1110 CHNS-O, Italy. Solution electrical conductivity measurements were done using an Elico type CM–82T (Hyderabad, India) conductivity bridge. Spectroscopic measurements were made using the following instruments: IR (KBr, 4000–600 cm^{-1}), Bruker Vector 22; electronic, Perkin Elmer Lambda 2 and Agilent 8453 diode-array spectrophotometer. ^{1}H NMR spectra ($CDCl_3$ solution) were obtained on Bruker WP-80 (80 MHz) spectrophotometer. Chemical shifts are reported in ppm referenced to TMS. X-Band EPR spectra on polycrystalline samples of **1–4** were performed with a Bruker ER 200 spectrometer, equipped with a helium continuous-flow cryostat.

Magnetism measurements

Magnetic susceptibility measurements on polycrystalline samples of **1–4** were carried out with a Superconducting Quantum Interference Design (SQUID) magnetometer in the temperature range 1.9–300 K, under an applied magnetic field of 0.01 Tesla for $T < 50$ K in order to avoid saturation effects and 1 Tesla for $T > 50$ K. Diamagnetic corrections were estimated from Pascal's constants.

X-Ray crystallography

Diffracted intensities were collected on a Bruker SMART APEX CCD diffractometer at 100(2) K (**2**) and at 293(2) K (**1**, **3** and **4**) using graphite-monochromated MoKα ($\lambda = 0.71073$ Å) radiation. Intensity data were corrected for Lorentz polarization effects. Empirical absorption correction (SADABS) was applied. The structures were solved by SIR-97, expanded by Fourier-difference syntheses and refined with SHELXL-97, incorporated in WinGX 1.64 crystallographic collective package.[14] Hydrogen atoms were placed in idealized positions, and treated using riding model approximation with displacement parameters derived from those of the atoms to which they were bonded. All non-hydrogen atoms were refined with anisotropic thermal parameters by full-matrix least-squares procedures on F^2. The convergence was measured by the factors R and R_w, where $R = \Sigma(||F_o| - |F_c||)/\Sigma|F_o|$ and $R_w = \{\Sigma[w(F_o^2 - F_c^2)^2]/\Sigma[w(F_o^2)^2]\}^{1/2}$. Pertinent crystallographic parameters are summarized in Table 1. For **3**, some degree of disorder was observed with solvent molecule MeCN. Two carbon atoms C(1S) and C(2S) were distributed over two positions and they were refined with site occupation factor of 0.55/0.45 and 0.50/0.50, respectively. Intermolecular contacts of C–H$\cdots\pi$ stacking and C–H$\cdots$O were examined with the DIAMOND

package.[15] C–H distances were normalized along the same vectors to the neutron derived values of 1.083 Å.[16]

The quality of the structure determination of **4** is poor, which is due to the poor quality of crystal chosen for data collection, and poor dataset obtained (see below).

Results and discussion

Synthesis and general characterization

The ligands $L^1(-)Li^+$, $L^2(-)Li^+$, $L^3(-)Li^+$ and $\{L^4(2-)(2Li^+)\}$ were synthesized by Michael condensation of methylacrylate with corresponding amines in MeOH, followed by hydrolysis of methyl esters. It should be mentioned here that very recently we have reported the synthesis of the ligands $L^1(-)Li^+$ and $L^2(-)Li^+$.[10] The new ligands $L^3(-)Li^+$ and $\{L^4(2-)(2Li^+)\}$ have been synthesized following a similar procedure and were characterized by their ^1H NMR spectra. The synthesis of four new complexes $\{[Ni^{II}(L^2)][ClO_4]\}_4\cdot MeCN$ (**1**), $\{[Cu^{II}(L^1)(O_3SCF_3)]\}_4\cdot H_2O$ (**2**), $\{[Cu^{II}(L^3)(OClO_3)]\}_4\cdot MeCN$ (**3**) and $\{[Cu^{II}(L^4)][ClO_4]\}_4\cdot 3MeCN\cdot 4H_2O$ (**4**) were achieved in H_2O by straightforward stoichiometric reactions between $[M^{II}(H_2O)_6]X_2$ ($M = Ni$, $X = ClO_4^-$; $M = Cu$, $X = CF_3SO_3^-$) and appropriate ligand. The synthesis of complexes **1–4** were based on the consideration that incorporation of carboxylate group in polydentate (2-pyridyl)alkylamine ligands will help in the self–assembly process and the formation of *syn–anti* carboxylate-bridged discrete coordination complexes. Our expectation was strengthened by our recent findings.[10] Identities of **1–4** were elucidated from physicochemical measurements [elemental analysis, IR and UV-vis spectra (Fig. S1 for **1** and Fig. S2–S4 for **2–4**)]† and X-ray crystal structure analysis (see below). Each complex displays in its IR spectra bands due to $\nu(COO^-)$ stretching vibration of coordinated carboxylate group at 1610 cm^{-1} and 1448 cm^{-1} for **1**; 1611 cm^{-1} and 1448 cm^{-1} for **2**; 1613 cm^{-1} and 1432 cm^{-1} for **3**; 1701, 1611 cm^{-1} and 1448 cm^{-1} for **4**. For complexes **1–4** the difference between $\nu_{as}(COO^-)$ and $\nu_{sym}(COO^-)$ stretching frequencies is near 170 cm^{-1}, thus suggesting a bridging coordination mode for the carboxylate group. The IR spectra also showed bands due to ionic/coordinated ClO_4^- for complexes **1**, **3** and **4** and due to coordinated $CF_3SO_3^-$ for **2**.

In MeCN all the complexes behave as 1 : 4 electrolyte.[12] Elemental analyses, IR and solution electrical conductivity data are in good agreement with the above formulations.

Crystal structure of $\{[Ni^{II}(L^2)][ClO_4]\}_4\cdot MeCN$ (1). The crystal structure of the complex $\{[Ni^{II}(L^2)][ClO_4]\}_4\cdot MeCN$ (**1**) consists of a tetranuclear unit $\{[Ni^{II}(L^2)][ClO_4]\}_4$. The complex is formed from four $\{Ni^{II}(L^2)\}^+$ units bridged by the carboxylate groups of the four tetradentate ligands. The immediate metal coordination environment is illustrated in Fig. 1. The ligand $L^2(-)$ acts as a tetradentate ligand towards Ni^{II} ions and as a monodentate bridging ligand towards a neighbouring Ni^{II} centre. Each Ni^{II} ion is coordinated by an ethylpyridyl nitrogen N(1), a methylpyridine nitrogen N(3), a tertiary amine nitrogen N(2), a carboxylate oxygen O(1) from the ligand $L^2(-)$ and an oxygen O(2) from another ligand from a neighbouring $\{Ni^{II}(L^2)\}^+$ unit. All the donor atoms of the ligand are thus utilized in the chelating and bridging mode for bonding with the Ni^{II} ions. All the Ni^{II} ions in this structure have equivalent coordination environment with similar geometric distortions, as a result of crystallographically-imposed symmetry. The carboxylate-bridging groups and four Ni^{II} ions form a 16-membered ring $(-Ni-O-C-O)_4$ with the metal ions located at the corners of an approximate square plane (see below). The $Ni\cdots Ni$ separations are ~6.25 Å along the two flattened edges and ~4.50 Å along the edges (the metal–metal distances are inclusive of van der Walls radii; it is true for **2–4** as well). The Ni^{II} centre assumes an ideal square-pyramidal geometry ($\tau = 0.001$).[17] Notably, each Ni^{II} ion is displaced by 0.2632 Å from the least-squares plane defined by the N_2O_2 basal plane towards the ethylpyridine nitrogen atom. Moreover, the axial Ni–N(1) bond is not perfectly perpendicular to the NiN_2O_2 plane but slightly bent off by 2.26°. Notably, the Ni–O(1)–C(16)–O(2#)–Ni# bridging network appreciably deviates from planarity [dihedral angle between the planes Ni–O(1)–C(16) and Ni#–O(2#)–C(16): 6.17(2)°] and the angle between the plane of the carboxylate group coordinated to Ni# and the NiN_3O plane is 84.512°.

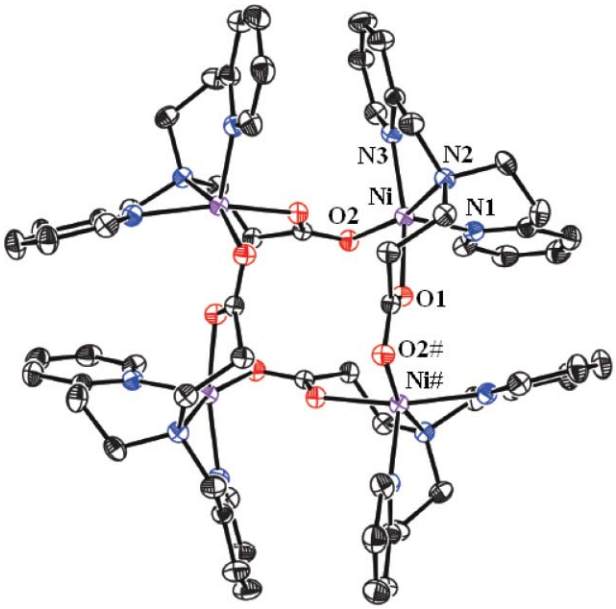

Fig. 1 View of the metal coordination environment in $\{[Ni^{II}(L^2)]^{4+}$ in the crystals of $\{[Ni^{II}(L^2)]\}_4[ClO_4]\cdot MeCN$ (**1**) at 30% thermal ellipsoids probability. Hydrogen atoms are omitted for clarity.

The Ni–N/O bond lengths around each Ni^{II} ion follow a usual pattern (Table 2). It should be pointed out here that in addition to five bonding interactions discussed above each Ni^{II} ion has a long Ni–O interaction at $Ni\cdots O(1) = 2.5334(7)$ Å. These distances are non-bonding, but the oxygen atoms are sterically placed to block the "sixth" coordination site in an "octahedral" arrangement of ligands around the metal ions. In essence, the ligand $L^2(-)$ is coordinated to Ni^{II} and folded in such a way that the tetranuclear structure was assembled, as reported with other carboxylate-based ligands.[18]

Crystal structure of $\{[Cu^{II}(L^1)(O_3SCF_3)]\}_4\cdot H_2O$ (2) and $\{[Cu^{II}(L^3)(OClO_3)]\}_4\cdot MeCN$ (3). The molecular structure of the complexes consist of tetranuclear motif $\{[Cu^{II}(L^1)(O_3SCF_3)]\}_4$/$\{[Cu^{II}(L^3)(OClO_3)]\}_4$. The complexes are formed from four $\{Cu(L^1)(O_3SCF_3)\}$/$\{Cu(L^3)(OClO_3)\}$ units bridged by the carboxylate groups of the four tridentate ligands. A general view

Table 2 Selected bond lengths (Å) and angles (°) in $\{[Ni^{II}(L^2)][ClO_4]\}_4 \cdot MeCN$ (**1**), $[Cu^{II}(L^1)(O_3SCF_3)]\}_4 \cdot H_2O$ (**2**) and $\{[Cu^{II}(L^3)(OClO_3)]\}_4 \cdot MeCN$ (**3**)

$\{[Ni^{II}(L^2)][ClO_4]\}_4 \cdot MeCN$ (**1**)			
Ni–O(1)	2.044(2)	O(1)–Ni–O(2)[a]	90.76(9)
Ni–O(2)[a]	2.037(2)	O(1)–Ni–N(1)	95.53(10)
Ni–N(1)	2.042(3)	O(1)–Ni–N(2)	93.35(10)
Ni–N(2)	2.083(3)	O(1)–Ni–N(3)	164.45(10)
Ni–N(3)	2.062(3)	O(2)[a]–Ni–N(1)	96.35(11)
C(16)–O(1)	1.274(4)	O(2)[a]–Ni–N(2)	164.36(10)
C(16)–O(2)	1.254(4)	O(2)[a]–Ni–N(3)	91.25(11)
Ni···Ni[a]	4.5006(11)	N(1)–Ni–N(2)	98.26(12)
		N(1)–Ni–N(3)	99.58(11)
		N(2)–Ni–N(3)	80.86(11)
		C(16)–O(1)–Ni	121.0(2)
		C(16)–O(2)–Ni[b]	103.3(2)
$\{[Cu^{II}(L^1)(O_3SCF_3)]\}_4 \cdot H_2O$ (**2**)			
Cu–O1	1.978(3)	O1–Cu–N1	170.78(12)
Cu–O2	1.997(3)	O1–Cu–N2	88.59(13)
Cu–O3	2.261(3)	O1–Cu–O2[a]	86.61(11)
Cu–N1	2.041(3)	O1–Cu–O3	90.69(11)
Cu–N2	2.014(3)	O2–Cu–N1	86.96(12)
C11–O1	1.263(5)	O2–Cu–N2	164.50(12)
C11[a]–O2	1.264(5)	O2–Cu–O3	90.35(11)
Cu···Cu[a]	4.527(6)	O3–Cu–N1	95.94(12)
		O3–Cu–N2	104.45(13)
		N1–Cu–N2	95.91(13)
		C11–O1–Cu	128.5(3)
		C11[a]–O2–Cu	106.6(2)
$\{[Cu^{II}(L^3)(OClO_3)]\}_4 \cdot MeCN$ (**3**)			
Cu–O1	1.929(3)	O1–Cu–N1	172.71(13)
Cu–O2[a]	1.997(3)	O1–Cu–N2	93.89(13)
Cu–O3	2.405(3)	O1–Cu–O2[a]	90.95(12)
Cu–N1	1.972(3)	O1–Cu–O3	103.09(11)
Cu–N2	2.060(4)	O2[a]–Cu–N1	89.78(13)
C12–O1	1.266(5)	O2[a]–Cu–N2	162.29(12)
C12–O2	1.261(5)	O2[a]–Cu–O3	90.07(11)
Cu···Cu[a]	4.524(6)	O3–Cu–N1	84.16(13)
		O3–Cu–N2	105.35(12)
		N1–Cu–N2	83.32(13)
		C12–O1–Cu	121.0(3)
		C12–O2–Cu[b]	108.0(3)

[a] Symmetry operators for the generated atoms: $-y + 1/2, x, -z + 3/2$ for **1**; $y + 1/2, -x + 1/2, -z + 1/2$ for **2** and $-y, x, -z$ for **3**. [b] Symmetry operators for the generated atoms: $y, -x + 1/2, -z + 3/2$ for **1**; $-y + 1/2, x - 1/2, -z + 1/2$ for **2** and $y, -x, -z$ for **3**.

of the complexes together with the formation of the carboxylate bridges and the immediate environment of the copper atoms is illustrated in Fig. 2 and Fig. S5†, respectively. All the Cu^{II} ions in these structures have equivalent coordination environment with similar geometric distortions (see below), due to crystallographic symmetry. The carboxylate-bridging groups and Cu^{II} ions form a 16-membered ring $(–Cu–O–C–O)_4$ with the four copper ions located at the corners of an approximate square plane (see below). The Cu···Cu separations are ~6.31/~6.26 Å along the two flattened edges and ~4.53/~4.52 Å along the edges for complexes **2** and **3**, respectively. Each copper ion is five-coordinate and bonded to two nitrogen and a carboxylate oxygen of the ligand, an oxygen atom of $CF_3SO_3^-/ClO_4^-$, and an oxygen atom of the carboxylate group from another ligand. All the donor atoms of the ligands are

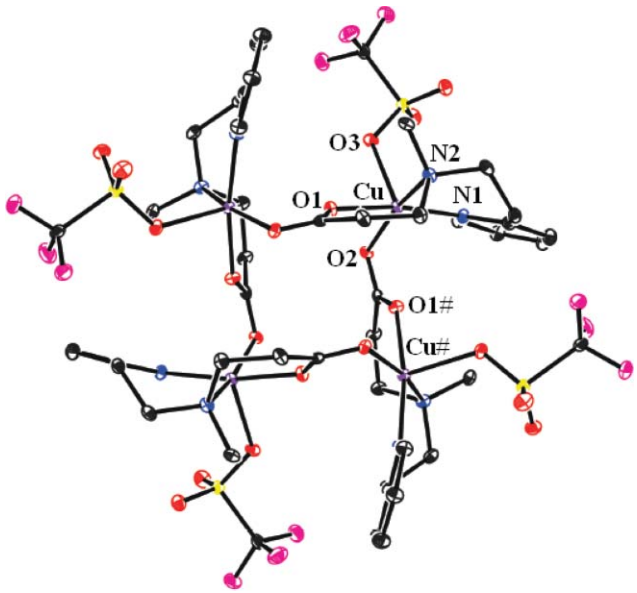

Fig. 2 View of the metal coordination environment in $\{[Cu^{II}(L^1)(O_3SCF_3)]\}_4$ in the crystals of $\{[Cu^{II}(L^1)(O_3SCF_3)]\}_4 \cdot H_2O$ (**2**) at 30% thermal ellipsoid probability. Hydrogen atoms are omitted for clarity.

thus utilized in the chelating and bridging modes of bonding with the Cu^{II} ions.

The coordination geometry around each copper may be described as slightly distorted square-pyramidal ($\tau = 0.100$) for **2** and ($\tau = 0.180$) for **3**, respectively.[17] The base of the pyramid is defined by three atoms N(1), N(2), O(1) from the same ligand and O(2) from another ligand, and the apical position is occupied by the O(3) from $CF_3SO_3^-/ClO_4^-$. The Cu^{II} ion is displaced by 0.1958/0.2069 Å from the least-squares plane defined by the N_2O_2 basal plane towards the O(3) oxygen of $CF_3SO_3^-/ClO_4^-$ in **2** and **3**, respectively. Notably, in **2** and **3** the Cu–O(2)–C(11)–O(1#)–Cu# and Cu–O(1)–C(12)–O(2#)–Cu(#) bridging network appreciably deviates from planarity [dihedral angle between the planes Cu–O(2)–C(11)/Cu–O(1)–C(12) and Cu#–O(1#)–C(11)/Cu#–O(2#)–C(12): 13.20(2)°/13.18(2)°] and the angle between the plane of the carboxylate group coordinated to Cu# and CuN_2O_2 plane is 84.160°/83.288°. The Cu–O(3) linkages are slightly bent off the perpendicular to the CuN_2O_2 plane by 7.74°/12.48° for complexes **2** and **3**, respectively. The Cu–N/O bond lengths around each copper in **2** and **3** are in the expected range. (Table 2).

It should be pointed out that as in **1** and $\{[Cu^{II}(L^1)][ClO_4]\}_4 \cdot MeCN$[10] both in **2** and **3**, each copper atom, in addition to the five bonding interactions discussed above, has a long Cu–O interaction at Cu···O(1) = 2.6557(1)/2.6639(6) Å. These distances are non-bonding, but the oxygen atoms are sterically placed to block the "sixth" coordination site in an "octahedral" arrangement of ligands around the metal ions. In essence, the ligands $L^1(–)$ and $L^3(–)$ are coordinated to Cu^{II} ions using all donor sites and folded in such a way that the tetranuclear structures were assembled, as reported with carboxylate-based ligands.[10,18]

Crystal structure of $\{[Cu^{II}(L^4)][ClO_4]\}_4 \cdot 3MeCN \cdot 4H_2O$ (4). As the quality of the structure determination of **4** is poor, the structure

was only partially determined.[19] Hence only the perspective view of the $\{[Cu^{II}(L^4)][ClO_4]\}_4$ core is displayed in Fig. 3.

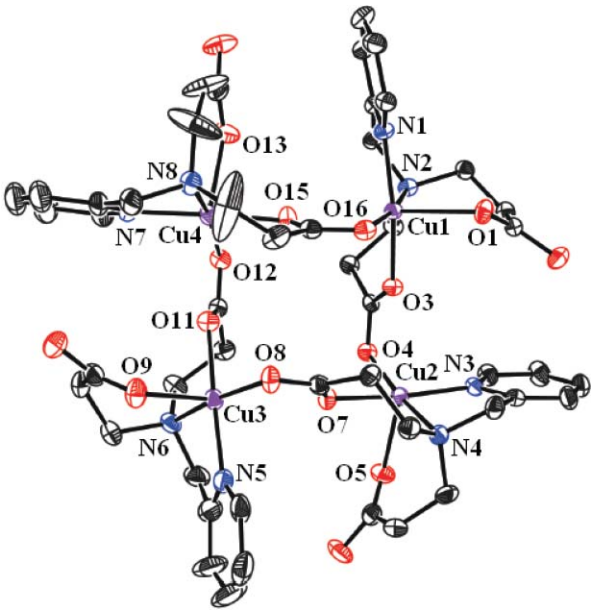

Fig. 3 View of the metal coordination environment in $\{[Cu^{II}(L^4)]\}_4^{4+}$ in the crystals of $\{[Cu^{II}(L^4)][ClO_4]\}_4 \cdot 3MeCN \cdot 4H_2O$ (**4**) at 30% thermal ellipsoids probability. Hydrogen atoms are omitted for clarity.

Nature of the geometry of four metal centres

It is appropriate to make a comment on the approximate geometry of the four metal centres (whether it is ideal/distorted square-planar or tetrahedral) in **1–4**. To address this question we consider the arrangement of four metal centres (Scheme 1), where D is the centroid of the four metal centre (Scheme 1). Given this the M–D–M angle is expected to be ~109.5° for ideal tetrahedral

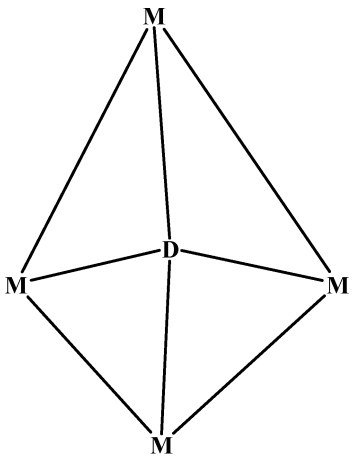

M = Ni, Cu

Scheme 1

arrangement and 90° for ideal square planar geometry. The corresponding values are 90.999(7)°/90.826(1)°/91.254(5)°/90.228(9)° for **1–4**, respectively. It clearly reveals that in the present complexes the four metal centres are close to an approximately square planar arrangement.

Non-covalent interactions

From careful analysis of the packing diagram it has been revealed that tetrameric Ni^{II} core of complex **1** is engaged in C–H···π interaction involving C–H of the pyridine ring in the equatorial plane and π cloud of the pyridine ring at the axial position (Fig. S6†). Complexes **2** and **3** are engaged in C–H···O interaction (Table S1†), involving the oxygen atom of Cu^{II}-bound $CF_3SO_3^-$ ion and methyl hydrogen atom of adjacent tetranuclear unit and the oxygen atom of Cu^{II}-bound ClO_4^- anion and methylene group of adjacent tetranuclear unit (Fig. 4), leading to the formation of 2D

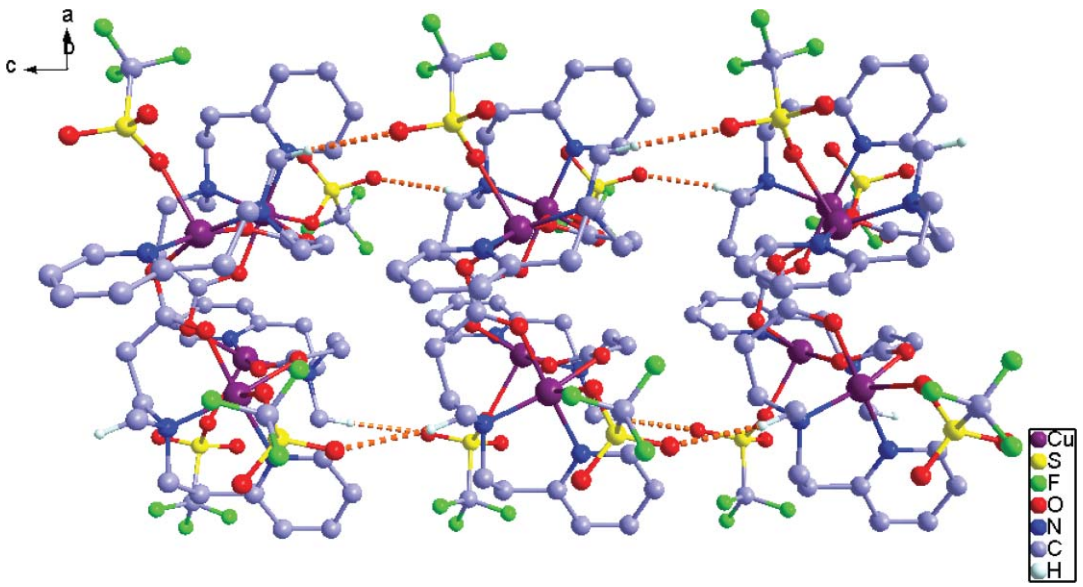

Fig. 4 Non-covalent (C–H···O) interaction involving tetranuclear complex $\{[Cu^{II}(L^1)(O_3SCF_3)]\}_4 \cdot H_2O$ (**3**).

network structures (Fig. S7†). The C–H···O hydrogen-bonding parameters observed in this work are in good agreement with prior results, including our own findings.[20–22] These can be classified as intermediate contacts (2.439–2.598 Å), which are appreciably shorter than the sum of the van der Waals radii for the H and the neutral O atoms (2.72 Å).[21] It is worth noting that complex **4** with bis-carboxylate-appended ligand is not involved in non-covalent interactions.

Magnetic properties

The global feature of the magnetic behaviour of **1–4** (Fig. 5 and 6) is characteristic of weak ferromagnetic exchange coupling between the four magnetic ions. At room temperature, the values of $\chi_M T$ correspond well with those expected for four quasi-non-interacting spin-triplets (**1**) or doublets (**2–4**). As seen in the plots, the values of the $\chi_M T$ product steadily increase as the temperature is lowered to reach maxima at 3.90, 4.8, 5.0 and 5.5 K for **1–4**, respectively, and then they decrease at lower temperatures. In principle, this decrease can be attributed to intermolecular antiferromagnetic interactions (θ), to zero-field splitting (D) effects within the ground spin states [$S = 4$ (**1**) and $S = 2$ (**2–4**)] or to both factors.

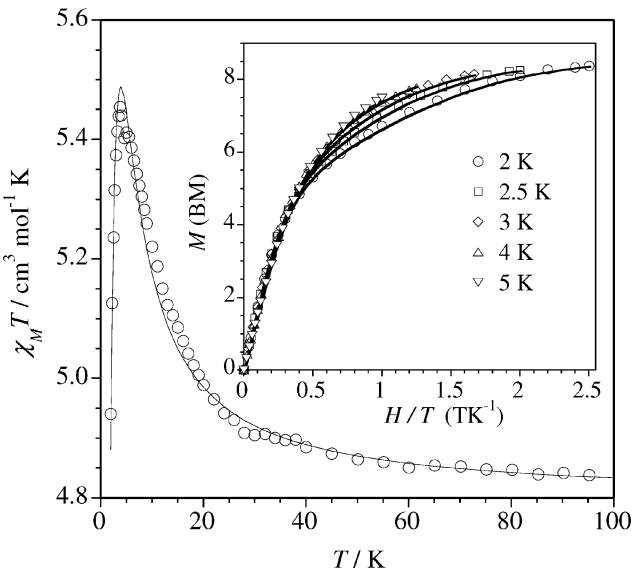

Fig. 5 Plot of $\chi_M T$ *vs.* T for a powdered sample of **1**. The inset sows the magnetization *vs.* applied field at 2.0, 2.5, 3.0, 4.0 and 5.0 K. The solid lines represent the best theoretical fits described in the text.

As shown in the crystallographic part, these complexes are made up of M_4 [M = Ni (**1**) and Cu (**2–4**)] entities where the carboxylato group of the ligand acts as a bridge in the *syn–anti* conformation to afford a square system (see Scheme 2). From such a Scheme, the spin Hamiltonian of the form of eqn (1) can be used to describe the magnetic properties of these compounds with $S = 1$ (**1**) and $S = 1/2$ (**2–4**).

$$H = -J(\hat{S}_1\hat{S}_2 + \hat{S}_2\hat{S}_3 + \hat{S}_3\hat{S}_4 + \hat{S}_1\hat{S}_4) - j(\hat{S}_1\hat{S}_3 + \hat{S}_2\hat{S}_4) \quad (1)$$

The energies of the low-lying states (E/J *vs.* the j/J ratio), deduced from the above Hamiltonian, with labelling according to C_4 point group,[23] are depicted in Fig. 7a and Fig. 8a. The theoretical expressions for the magnetic susceptibility per

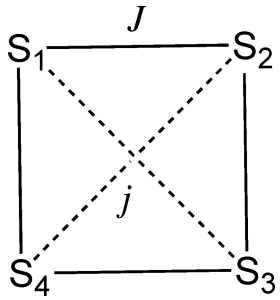

Scheme 2

each M_4 unit obtained from the above energy levels are given by eqn (A1) and (A2).

$$\chi_M = \frac{2N\beta^2 g^2}{k(T-\theta)}\left\{\frac{A}{Z}\right\};\ \text{where}\ x = -\frac{J}{kT}\ \text{and}\ y = -\frac{j}{kT}$$
$$A = A_1 + A_2$$
$$Z = Z_1 + Z_2 + Z_3$$
$$A_1 = \exp(9x) + 5\exp(7x) + \exp(7x+2y) + 5\exp(5x+2y) + \exp(5x+4y) + 14\exp(4x)$$
$$A_2 = 5\exp(4x+3y) + \exp(4x+5y) + 5\exp(3x+4y) + 14\exp(2x+2y) + 30 \quad (A1)$$
$$Z_1 = \exp(10x) + 3\exp(9x) + 5\exp(7x) + 6\exp(7x+2y) + \exp(6x+4y) + 10\exp(5x+2y)$$
$$Z_2 = 3\exp(5x+4y) + 7\exp(4x) + 10\exp(4x+3y) + 6\exp(4x+5y) + \exp(4x+6y)$$
$$Z_3 = 5\exp(3x+4y) + 14\exp(2x+2y) + 9$$

$$\chi_{\parallel} = \frac{2N\beta^2 g_{\parallel}^2}{k(T-\theta)}\left\{\frac{F_D^{\parallel} + F_J}{Z}\right\}$$
$$\chi_{\perp} = \frac{2N\beta^2 g_{\perp}^2}{k(T-\theta)}\left\{\frac{F_D^{\perp} + F_J}{Z}\right\} \quad (A2)$$
$$\chi_M = \frac{\chi_{\parallel} + 2\chi_{\perp}}{3}$$

where

$$Z = Z_D + Z_J$$
$$Z_D = \exp(+2D/kT) + 2\exp(D/kT) + 2\exp(-2D/kT)$$
$$Z_J = 5 + \exp[-(J+2j)/kT] + 6\exp[-(J+j)/kT] + 3\exp(-2J/kT) + \exp(-3J/kT)$$
$$F_J = 2\exp[-(J+j)/kT] + \exp(-2J/kT)$$
$$F_D^{\parallel} = \exp(+D/kT) + 4\exp(-2D/kT)$$
$$F_D^{\perp} = \frac{kT}{3D}[9\exp(+2D/kT) - 7\exp(+D/kT) - 2\exp(-2D/kT)]$$

It is seen in Fig. 7 and 8 that the low-lying level is $S = 4$ [^{9}A, (**1**)] or $S = 2$ [^{5}B, (**2–4**)] when $J > 0$ and $j/J > -2/3$ or $j/J > -1/2$, respectively. Due to the fact that the value of the j parameter is expected to be very small ($j << J$) this exchange pathway cannot be responsible for the decrease of the values of $\chi_M T$ at low temperature. In fact, reasonable fit cannot be achieved by using eqn (A1) and (A2) with J, j and g as the variable parameters ($D = 0$ and $\theta = 0$). So, the j parameter is most likely negligible.

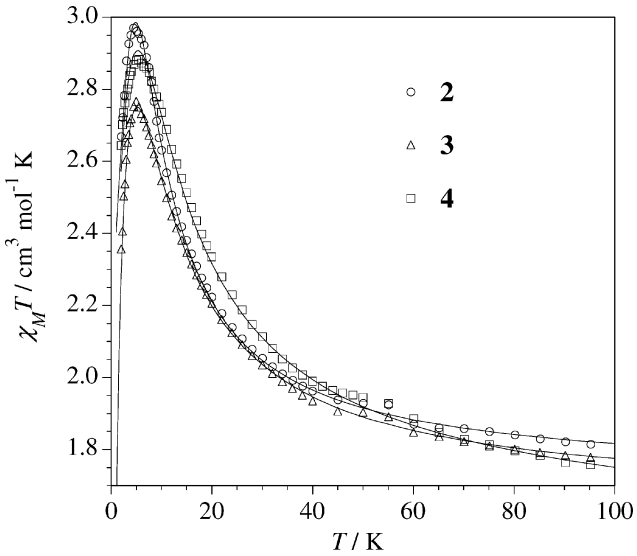

Fig. 6 Plot of $\chi_M T$ *vs.* T for powdered samples of **2–4**. The solid lines represent the best theoretical fits described in the text.

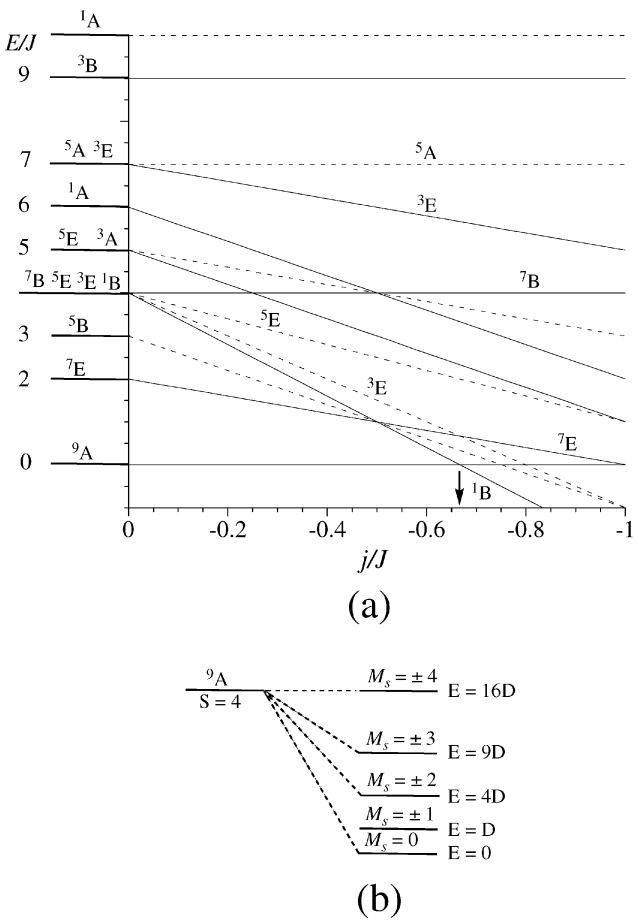

Fig. 7 (a) Energy diagram for **1** showing the low-lying states (E/J *vs.* j/J ratio), deduced from Hamiltonian in the form of eqn (1), with labelling according to C_4 point group. (b) Zero-field splitting of the nonet ground spin-state ($S = 4$).

Assuming that the decrease of $\chi_M T$ is mainly due to the zero-field splitting (zfs) effects, and given the fact that the Ni^{II} ion can

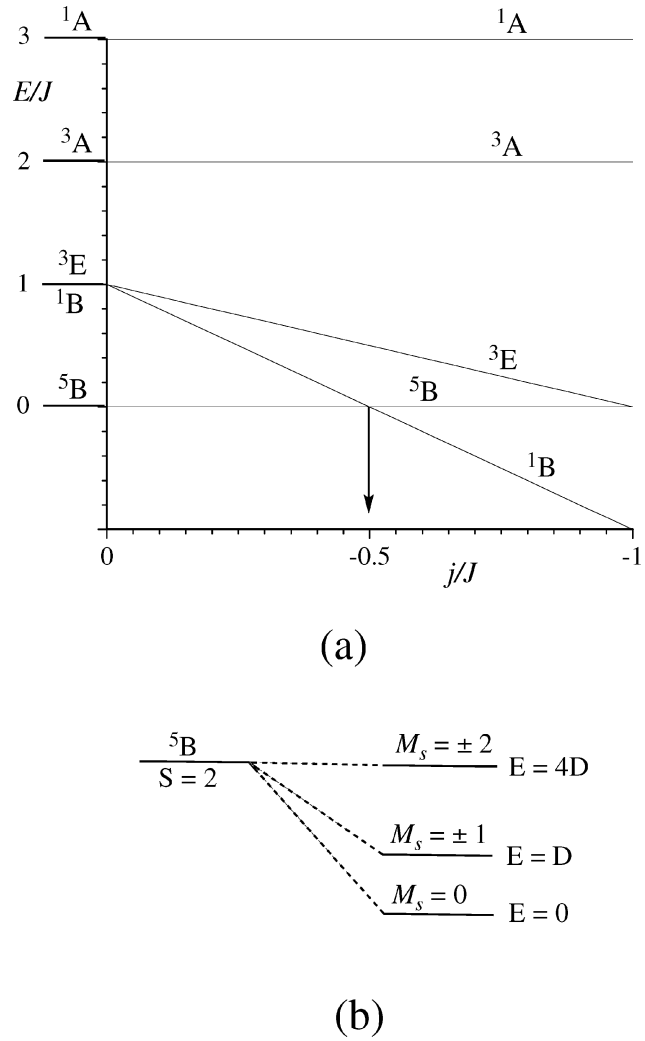

Fig. 8 (a) Energy diagram for **2–4** showing the low-lying states (E/J *vs.* j/J ratio), deduced from Hamiltonian in the form of eqn (1), with labelling according to C_4 point group. (b) Zero-field splitting of the quintet ground spin-state ($S = 2$).

exhibit an important zfs, we introduce this effect by using the Hamiltonian of the form of eqn (2) together with the Hamiltonian of the form of eqn (1), where the D parameter is the axial zfs for each Ni^{II} ion.

$$H_{zfs} = \sum_{i=1}^{4} D(S_{zi}^2 - 2/3) \quad (2)$$

As for this case, an analytical expression for the magnetic susceptibility cannot be derived, numerical matrix diagonalisation techniques through a FORTRAN program[24] were used in the fitting procedure. The best-fit parameters are $g = 2.18$, $D_{Ni} = 3.9$ cm^{-1} and $J = 0.62$ cm^{-1}. We can estimate the value of the D parameter for the nonet[25] ($S = 4$) ground spin-state, $D_{S=4} = (1/7)D_{Ni} = 0.56$ cm^{-1}. This value is of the same order of magnitude as J. As shown in Fig. 7b, the width of the zfs is large (16 $D_{S=4} = 8.9$ cm^{-1}) mixing thus the excited spin-states.

In order to determine more accurately the D parameter, we measured the magnetization of **1** as a function of applied field (H) at different temperatures. The experimental data thus obtained were fitted by means of the Hamiltonians in the forms of eqn (1)

and eqn (2). The best-fit parameters are $g = 2.18$, $J = 1.2$ cm^{-1} and $D_{Ni} = 3.34$ cm^{-1}. The larger value of D_{Ni} determined from magnetic susceptibility measurements ($D_{Ni} = 3.9$ cm^{-1}) may be attributed to the presence of intermolecular magnetic interactions. A fit of the magnetic susceptibility data, keeping $D_{Ni} = 3.34$ cm^{-1} constant and introducing a parameter θ (see above), yielded $J = 1.0$ cm^{-1}, $g = 2.18$ and $\theta = -0.8$ K. Notably, the X-band EPR spectra of a powdered sample of **1** are silent in the temperature range (4–300 K), supporting the occurrence of a zfs with $D_{S=4} > h\nu \approx 0.3$ cm^{-1}.

In the case of the Cu^{II} complexes (**2–4**) without local zfs ($D_{Cu} = 0$), the zfs of the quintet ground spin-state ($S = 2$), which would be due to the dipolar and anisotropic interactions,[25,26] is expected to be small. So, assuming that the decrease of $\chi_M T$ in **2–4** is mainly due to the zfs effects of the quintet (see Fig. 8b) and this state is well separated in energy from the next excited spin-states (*i.e.*, $D_{S=2} << J$), the eqn (A2) can be deduced for the magnetic susceptibility to describe the magnetic behaviour of **2–4**. The best-fit parameters are $g = 2.11$, $D_{S=2} = 0.3$ cm^{-1} and $J = 10.9$ cm^{-1} for **2**, $g = 2.10$, $D_{S=2} = 0.4$ cm^{-1} and $J = 11.1$ cm^{-1} for **3**, and $g = 2.07$, $D_{S=2} = 0.35$ cm^{-1} and $J = 13.4$ cm^{-1} for **4**. The low value of the D/J ratio (*ca.* 0.03) allows the use of eqn (A2).

As indicated above, the decrease of $\chi_M T$ at low temperatures could also be attributed to the intermolecular interactions. In this sense, we can reproduce the $\chi_M T$ curve by using a Weiss constant (θ) in the form of $(T - \theta)$. The fit through eqn (A2) with $D = 0$ for **2–4** leads to the same values of J and g, θ being –0.4, –0.6 and –0.5 K, respectively.

The J values obtained here are comparable to reported systems of similar structural type.[26] In all these systems the carboxylato bridge with *syn–anti* conformation offers ferromagnetic interactions. As shown in Scheme 3, the magnetic orbitals are unfavourably oriented to give a significant overlap and so, a ferromagnetic interaction is observed. The non-planarity of the M–O–C–O–M bridging network also contributes to reduce the overlap and thus increasing the ferromagnetic coupling. All these features have been analyzed through DFT calculations for Cu^{II} complexes for different conformation of the carboxylate bridge.[27] In fact, the calculated coupling constant by the authors of this report for the *syn–anti* mode is about 10 cm^{-1}, in a very good agreement with our experimental results.

EPR spectra

The EPR spectra of powdered samples of tetranuclear Cu^{II} complexes **2–4** at different temperatures are shown in Fig. 9. At room temperature and even at 120 K, each complex shows an intense, almost isotropic, featureless resonance at $g = 2.14$, 2.12 and 2.13 for **2–4**, respectively. As the temperature is lowered down to 4.0 K, a very weak axial anisotropy is observed. These features clearly show that the zfs of the quintet ground spin state ($S = 2$) of **2–4** is very small, $D_{S=2} << h\nu \approx 0.3$ cm^{-1}.[28] So, the decrease of the $\chi_M T$ values at low temperatures for all these tetracopper(II) complexes has to be attributed to intermolecular interactions.

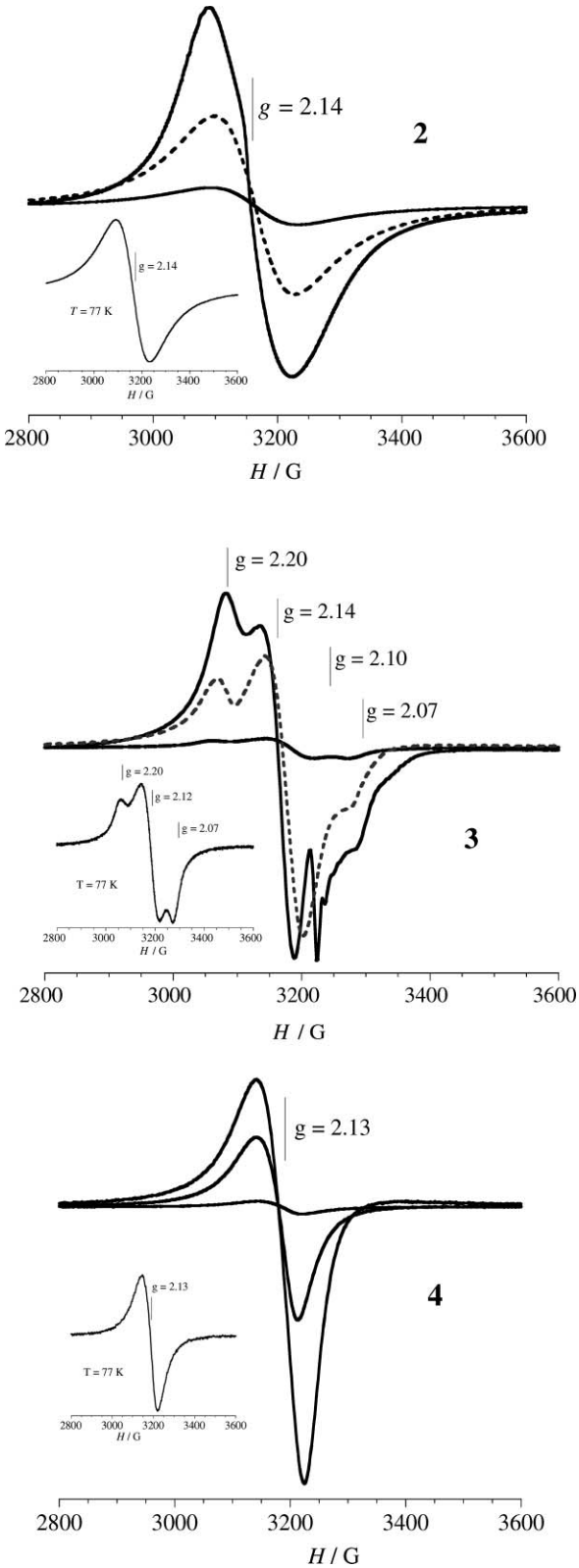

Fig. 9 X-Band EPR spectra of polycrystalline samples of **2–4** at 77, 10 and 4 K.

Rationalization of observed magnetic behaviour

The magnetic-exchange interactions in $\{[Cu^{II}(L^1)(OClO_3)]\}_4 \cdot MeCN$[10] and **2–4** are strong because the carboxylate bridge links two adjacent equatorial positions (Scheme 3). In order to understand the different nature of the magnetic exchange interactions in these Cu^{II}_4 complexes (ferromagnetic) it is important

Table 3 Magnetostructural data for Cu–O–C–O–Cu# fragment

Complex	β/°[a]	α/°[b]	Cu–O–C–O–Cu#	τ	g	J/cm^{-1}	D/cm^{-1}
$\{[Cu^{II}(L^1)][ClO_4]\}_4$·MeCN[10]	89.32	71.77	4.99(5)	0.10	2.08	12.2	0.80
2	84.16	68.65	13.20(2)	0.10	2.11	10.9	0.30
3	83.29	71.84	13.18(2)	0.18	2.10	11.1	0.40
4	86.15	73.86	7.08(4)	0.06	2.07	13.4	0.35

[a] At each copper centre, the value of the dihedral angle between the plane of the carboxylate group and the basal plane. [b] Scheme 4.

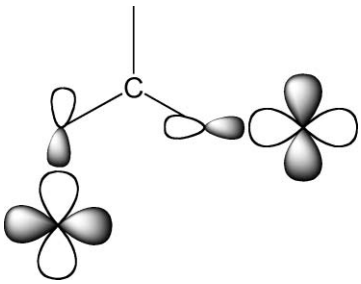

Scheme 3

to take into account the fact that the *syn–anti* carboxylate bridge mediates weak magnetic-exchange interactions, either ferro- or antiferromagnetic (Table 3).[18a,b,d,f] From this perspective, the Scheme 4 is illustrative: when the α value is close to 90° a ferromagnetic exchange interaction is expected, while smaller values for this angle lead to an antiferromagnetic coupling. In fact, the prediction is in conformity with the observed values of α (~71.77° for $\{[Cu^{II}(L^1)(OClO_3)]\}_4$·MeCN,[10] 68.65° for **2**, 71.84° for **3** and ~73.86° for **4**). The out-of-plane deviations in the M–O–C–O$^{\#}$–M$^{\#}$ skeleton (see above) also play a relevant role.

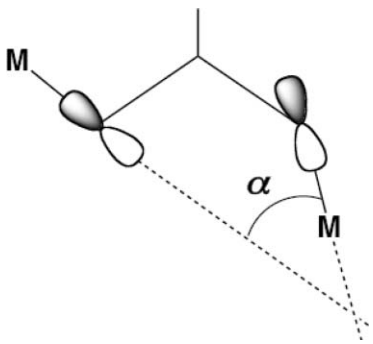

Scheme 4

Summary and conclusions

In this work four new complexes [one discrete tetranickel(II) cluster and three discrete tetracopper(II) clusters] supported by carboxylate-appended (2-pyridyl)alkylamine ligands have been structurally and magnetically characterized. Crystal packing diagrams reveal 2D architecture construction *via* C–H$\cdots\pi$ and C–H$\cdots$O interactions. Temperature-dependent magnetic susceptibility measurements reveal ferromagnetic exchange interaction in all the complexes. The successful syntheses of these complexes enriched the *syn–anti* carboxylate-bridged complexes not only structurally but magnetically as well. Future efforts will investigate how the stereochemical demand of this class of ligands would direct the molecular shape and control the magnetic properties of the resulting complexes. Such an endeavour is ongoing in this laboratory.

Acknowledgements

This work is supported by the Department of Science & Technology, Government of India and by the Ministerio de Educación y Ciencia (MEC, Spain; projects CTQ2007–61690 and Consolider-Ingenio in Molecular Science CSD2007-00010). RM is thankful to the DST for a J C Bose Fellowship. HA gratefully acknowledges the award of SRF by Council of Scientific & Industrial Research, Government of India.

References

1 O. Kahn, *Molecular Magnetism*, VCH publishers, Weinheim, Germany, 1993.
2 O. Kahn, *Adv. Inorg. Chem.*, 1995, **43**, 179.
3 K. S. Murray, *Adv. Inorg. Chem.*, 1995, **43**, 261.
4 (*a*) C. Ruiz-Pérez, Y. Rodríguez-Martín, M. Hernández-Molina, F. S. Delgado, J. Pasán, J. Sanchiz, F. Lloret and M. Julve, *Polyhedron*, 2003, **22**, 2111; (*b*) J. Pasán, F. S. Delgado, Y. Rodríguez-Martín, M. Hernández-Molina, C. Ruiz-Pérez, J. Sanchiz, F. Lloret and M. Julve, *Polyhedron*, 2003, **22**, 2143; (*c*) K.-Y. Choi, Y.-M. Jeon, H. Ryu, J.-J. Oh, H.-H. Lim and M.-W. Kim, *Polyhedron*, 2004, **23**, 903; (*d*) S.-i. Noro, H. Miyasaka, S. Kitagawa, T. Wada, T. Okubo, M. Yamashita and T. Mitani, *Inorg. Chem.*, 2005, **44**, 133; (*e*) K.-Y. Choi, S.-Y. Park, Y.-M. Jeon and H. Ryu, *Struct. Chem.*, 2005, **16**, 649; (*f*) J. Pasán, J. Sanchiz, C. Ruiz-Pérez, F. Lloret and M. Julve, *Inorg. Chem.*, 2005, **44**, 7794; (*g*) Y.-Z. Zheng, M.-L. Tong, W.-X. Zhang and X.-M. Chen, *Angew. Chem., Int. Ed.*, 2006, **45**, 6310; (*h*) L. Caadillas-Delgado, O. Fabelo, J. Pasn, F. S. Delgado, F. Lloret, M. Julve and C. Ruiz-Prez, *Inorg. Chem.*, 2007, **46**, 7458.
5 (*a*) G. B. Deacon and R. J. Phillips, *Coord. Chem. Rev.*, 1980, **33**, 227; (*b*) M. Melnik, *Coord. Chem. Rev.*, 1981, **36**, 1; (*c*) M. Kato and Y. Muto, *Coord. Chem. Rev.*, 1988, **92**, 45; (*d*) E. Colacio, J. M. Domínguez-Vera, M. Ghazi, R. Kivekäs, M. Klinga and J. M. Moreno, *Eur. J. Inorg. Chem.*, 1999, 441, and references therein.
6 C. Oldham, In *Comprehensive Coordination Chemistry*, G. Wilkinson, R. D. Gillard and J. A. McCleverty, ed., Pergamon Press, Oxford, U.K., 1987, vol. 2, p. 435.
7 R. J. Doedens, *Prog. Inorg. Chem.*, 1976, **21**, 209.
8 S. J. Rettig, R. C. Thompson, J. Trotter and S. Xia, *Inorg. Chem.*, 1999, **38**, 1360, and references therein.
9 V. Tangoluis, G. Psomas, C. Dendrinou-Samara, C. P. Raptopoulou, A. Terzis and D. P. Kessissoglou, *Inorg. Chem.*, 1996, **35**, 7655.
10 H. Arora, F. Lloret and R. Mukherjee, *Inorg. Chem.*, 2009, **48**, 1158.
11 (*a*) S. Bhattacharya, K. Snehalatha and V. P. Kumar, *J. Org. Chem.*, 2003, **68**, 2741; (*b*) N. M. F. Carvalho, A. Jr. Horn, R. B. Faria, A. J. Bortoluzzi, V. Drago and O. A. C. Antunes, *Inorg. Chim. Acta*, 2006, **359**, 4250.
12 W. J. Geary, *Coord. Chem. Rev.*, 1971, **7**, 81.
13 (*a*) F. A. Cotton, G. Wilkinson and M. Bochmann, *Advanced Inorganic Chemistry*, Wiley, New York, 6th edn 1999; (*b*) Y.-S. Dou, *J. Chem. Educ.*, 1990, **67**, 134; (*c*) B. J. Hathaway, *Struct. Bonding*, 1984, **57**, 55.

14 L. J. Farrugia, WinGX version 1.64, *An Integrated System of Windows Programs for the Solution, Refinement and Analysis of Single-Crystal X-ray Diffraction Data*, Department of Chemistry, University of Glasgow, 2003.
15 K. Brandenburg, *DIAMOND ver 2.1c*, Crystal Impact GbR, Bonn, Germany, 1999.
16 T. Steiner, *Angew. Chem., Int. Ed.*, 2002, **41**, 48.
17 A. W. Addison, T. N. Rao, J. Reedijk, J. van Rijn and G. C. Verschoor, *J. Chem. Soc., Dalton Trans.*, 1984, 1349.
18 (*a*) Selected examples of carboxylato-bridged tetracopper(II) complexes: E. Colacio, J.-P. Costes, R. Kivekäs, J.-P. Laurent and J. Ruiz, *Inorg. Chem.*, 1990, **29**, 4240; (*b*) E. Colacio, J.-M. Dominguez-Vera, J.-P. Costes, R. Kivekäs, J.-P. Laurent, J. Ruiz and M. Sundberg, *Inorg. Chem.*, 1992, **31**, 774; (*c*) S. Wang, S. J. Trepanier, J.-C. Zheng, Z. Pang and M. J. Wagner, *Inorg. Chem.*, 1992, **31**, 2118; (*d*) E. Colacio, M. Ghazi, R. Kivekäs and J. M. Moreno, *Inorg. Chem.*, 2000, **39**, 2882; (*e*) M. Murugesu, R. Clérac, B. Pilawa, A. Mandel, C. E. Anson and A. K. Powell, *Inorg. Chim. Acta*, 2002, **337**, 328; (*f*) S. K. Dey, B. Bag, K. M. Abdul Malik, M. Salah El Fallah, J. Ribas and S. Mitra, *Inorg. Chem.*, 2003, **42**, 4029.
19 Crystal data for **4**. $C_{54}H_{48}Cl_4Cu_4N_{11}O_{36}$, $M = 1822.99$, triclinic, space group $P1\bar{1}$ (no. 2), $a = 10.960(5)$, $b = 14.823(5)$, $c = 25.883(5)$ Å, $\alpha = 76.241(5)$, $\beta = 87.467(5)$, $\gamma = 68.532(5)°$, $U = 3797(2)$ Å^3, $Z = 2$, $D_{calcd} = 1.595$ g cm^{-3}, $\mu(\mathrm{MoK}\alpha) = 1.342$ mm^{-1}, 25 319 reflections measured, 18 004 unique, and 8824 ($>4\sigma(I)$) used in the calculations; $T = 293(2)$ K, final $R = 0.0895$, w$R = 0.2348$.
20 R. Taylor and O. Kennard, *J. Am. Chem. Soc.*, 1982, **104**, 5063.
21 L. Brammer in *Perspectives in Supramolecular Chemistry—Crystal Design: Structure and Function*, G. R. Desiraju, Ed., vol. 7, Wiley, Chichester, 2003, pp. 1.
22 (*a*) V. Balamurugan, M. S. Hundal and R. Mukherjee, *Chem.–Eur. J.*, 2004, **10**, 1683; (*b*) H. Mishra and R. Mukherjee, *J. Organomet. Chem.*, 2006, **691**, 3545.
23 B. Tsukerblat, *Inorg. Chim. Acta*, 2008, **361**, 3746.
24 J. Cano, *VPMAG, Revision C03*, University of València, Spain, 2004.
25 A. Bencini and D. Gatteschi, *Electron Paramagnetic Resonance of Exchange Coupled Systems*, Springer-Verlag, Berlin Heidelberg, 1990.
26 (*a*) Y. Rodriguez-Martín, C. Ruiz-Pérez, J. Sánchiz, F. Lloret and M. Julve, *Inorg. Chim. Acta*, 2001, **318**, 159; (*b*) Y. Rodriguez-Martín, M. Hernández-Molina, F. S. Delgado, J. Pasán, C. Ruiz-Pérez, J. Sánchiz, F. Lloret and M. Julve, *CrystEngComm*, 2002, **4**, 522; (*c*) Y. Rodriguez-Martín, M. Hernández-Molina, F. S. Delgado, J. Pasán, C. Ruiz-Pérez, J. Sánchiz, F. Lloret and M. Julve, *CrystEngComm*, 2002, **4**, 440; (*d*) F. S. Delgado, J. Sánchiz, C. Ruiz-Pérez, F. Lloret and M. Julve, *Inorg. Chem.*, 2002, **26**, 1624; (*e*) J. Sánchiz, Y. Rodriguez-Martín, C. Ruiz-Pérez, A. Mederos, F. Lloret and M. Julve, *New J. Chem.*, 2003, **42**, 5938.
27 A. Rodríguez-Fortea, P. Alemany, S. Alvarez and E. Ruiz, *Chem.–Eur. J.*, 2001, **7**, 627.
28 F. E. Mabbs and D. Collison, *Electron Paramagnetic Resonance of d Transition Metal Compounds*, Elsevier Science Publishers B. V., 1992.